One-Dimensional Magnetism in New, Layered Structures: Piperazine-Linked Copper and Nickel Oxalate Chains

Tony D. Keene,[a] Helen R. Ogilvie,[a] Michael B. Hursthouse,[a] and Daniel J. Price*[a]

Keywords: Magnetic properties / Layered compounds / Hydrothermal synthesis / Coordination networks

Two new coordination network materials with the composition M(pip)(ox) (pip = piperazine; ox = oxalate; M = Ni, Cu) have been synthesised under ambient and hydrothermal conditions. These compounds adopt related structures, both consisting of intersecting $[M(pip)]_\infty$ and $[M(ox)]_\infty$ chains, which result in layered structures. The nickel compound crystallises in $P\bar{1}$. The metal ions are octahedrally coordinated and are linked by symmetric chelating bridging oxalate ions. In contrast, the copper compound crystallises in the chiral space group $P2_12_12_1$. Here the copper atom displays square pyramidal coordination geometry and the oxalate ions bridge metals in an unsymmetric fashion resulting in a polar metal-oxalate chain structure. The magnetic behaviour is determined by the nature of the exchange-coupled network. Only the antiferromagnetic interaction mediated by the bridging oxalate group is significant and the compounds are well modelled as 1-D antiferromagnetically coupled chains. For the copper compound ($S = {}^1/_2$) we determined J/k_B to be −25.9 K, while the nickel compound ($S = 1$) shows a larger exchange coupling ($J/k_B = -42.2$ K). In the nickel compound we see a significant deviation between the observed and calculated magnetic susceptibilities at the lowest experimental temperatures. This may be due either to the formation of a Haldane quantum antiferromagnetic ground state or to single-ion zero-field splitting effects.

(© Wiley-VCH Verlag GmbH & Co. KGaA, 69451 Weinheim, Germany, 2004)

Introduction

Structurally, the oxalate anion is well-known for its chelating coordination mode and for its symmetric bis-chelating bridging mode. The prevalence of this linking mode provides a degree of predictability with regard to the structural motifs and the architectures found in oxalate coordination networks.[1] Electronically, the oxalate anion is very good at mediating an exchange interaction between bridged paramagnetic metal ions. Consequently, many 1-D,[2] 2-D[3] and 3-D[4] magnetic networks have been characterised that contain just this bridging mode.

Magnetostructural correlations in oxalate-bridged homometallic Ni^{II} [5] and Cu^{II} [6] compounds are well-known. For Ni^{II}, the most common geometry; octahedral coordination and a symmetric bis-chelating oxalate bridge, results in antiferromagnetic coupling interactions in the range;(J/k_B = −32 to −56 K). The variation can be correlated with the coordination environment of the nickel ion. By comparison, oxalate-bridged copper-containing compounds show a greater range of coupling constants (0 to −500 K). Here the d^9 configuration means that only one magnetic orbital on each metal is involved in the coupling interaction. Thus, the symmetry of the crystal field and the relative orientations of the local crystal field axis of neighbouring metals to the bridging group orbitals are the key in determining the sign and magnitude of the magnetic interaction. The range of coupling constants is related to the variety of coordination geometries adopted by Cu^{II} ions.

In terms of structure, while many dinuclear oxalate-bridged nickel compounds are known, relatively few infinite chain structures have been reported.[7] This may be in part due to the difficulty in crystallising low solubility network materials. Similarly, symmetrically bridged dinuclear copper compounds are much more prevalent than other mono or polynuclear complexes. However, there are many more extended copper oxalate chain structures than analogous nickel structures.[8] In addition we see examples of 2-D networks[9] in solid-state copper oxalate chemistry. Although the symmetric bridging mode is dominant, there is a much greater variability in the oxalate coordination by copper, resulting in a greater range of oxalate bridging modes.

We have initiated a program of research to use structure-directing amines and ammonium cations in the synthesis of new oxalate network structures. Here we present the synthesis, structure and magnetic properties of two new compounds both with the composition M(pip)(ox) (e.g. where M is either Ni (**1**) or Cu (**2**), pip is the neutral cyclic diamine, piperazine and ox is the oxalate dianion. Our choice of oxalate and piperazine as distinct types of predominantly linear bridging ligands result in straight-forward network topologies in **1** and **2**. Despite the similarity in composition and overall structure, **1** and **2** crystallise in different space

[a] School of Chemistry, University of Southampton, Highfield, Southampton, SO17 1BJ, United Kingdom
Fax: (internat.) + 44-2380-596805
E-mail: daniel.price@soton.ac.uk

groups with different structures and very different metal and oxalate coordination environments.

Results and Discussion

Crystal Structures

Crystallographic data for both compounds are given in Table 1. The asymmetric unit of **1** (Figure 1) contains one half of a nickel atom, one half of a piperazine molecule and one half of an oxalate dianion. All of these components lie on crystallographic inversion centres. The nickel ion is approximately octahedrally coordinated with a *trans*-N_2O_4 coordination sphere. The oxalate ions chelate and bridge adjacent nickel ions in a normal fashion resulting in linear chains of metal oxalate running parallel to the *a*-axis [Figure 2 (a)]; thus the Ni···Ni separation in these chains is the *a*-parameter [5.3613(11) Å]. Two nickel ions are linked by a piperazine molecule, in the low-energy chair form, with bonds to the equatorial position. Thus the nickel ions and the piperazines form another 1-D motif, this time running parallel to the [01$\bar{1}$] direction with a Ni···Ni separation of 7.225(41) Å. Together the bridging oxalate and piperazine groups connect the nickel ions into a 2-D net in the (011) plane [Figure 2 (b)]. While the shortest Ni···Ni separation

Table 1. Crystallographic data for Ni(pip)(ox) (**1**) and Cu(pip)(ox) (**2**)

Compound	**1**	**2**
Formula	$C_6H_{10}N_2NiO_4$	$C_6H_{10}CuN_2O_4$
Crystal system	triclinic	orthorhombic
Space group	$P\bar{1}$ (no. 2)	$P2_12_12_1$ (no. 19)
a (Å)	5.3632(11)	6.8678(3)
b (Å)	5.9848(14)	10.3459(5)
c (Å)	6.4997(16)	10.6329(6)
α (°)	70.584(8)	90
β (°)	85.498(9)	90
γ (°)	78.176(12)	90
V (Å^3)	192.57(72)	755.51(7)
ρ (g cm^{-3})	2.008	2.090
T (K)	120	298
μ (mm^{-1})	2.500	2.872
Reflections collected	1271	5587
Unique data/parameters	776/63	1733/128
R_{int}	0.0765	0.0470
Goodness of fit (*S*)	1.040	1.185
*R*1/*wR*2 [$I > 2\sigma(I)$]	0.0562/0.1253	0.03760.0932
*R*1/*wR*2 [all data]	0.0760/0.1253	0.0436/0.1156

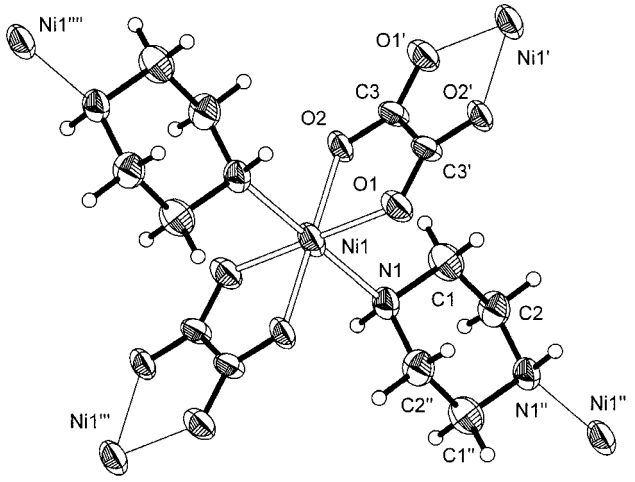

Figure 1. The asymmetric unit and selected symmetry equivalents of Ni(pip)(ox) (**1**) showing the nickel coordination sphere and the bridging modes of both ligands; thermal ellipsoids are at the 90 % probability level; selected bond lengths (Å) and angles (°): Ni1−O1 2.060(11), Ni1−O2 2.065(8), Ni1−N1 2,184(13), C3−C3′ 1.555(5), C3−O1′ 1.257(4), C3−O2 1.253(5) Å; O1−Ni1−O2 81.49(1), O1−Ni1−N1 88.69(1), O2−Ni1−N1 90.80(1)°; symmetry codes: ′ $(1-x, -y, -z)$; ′′ $(-x, 1-y, -1-z)$; ′′′ $(-1+x, y, z)$; ′′′′ $(x, -1+y, 1+z)$

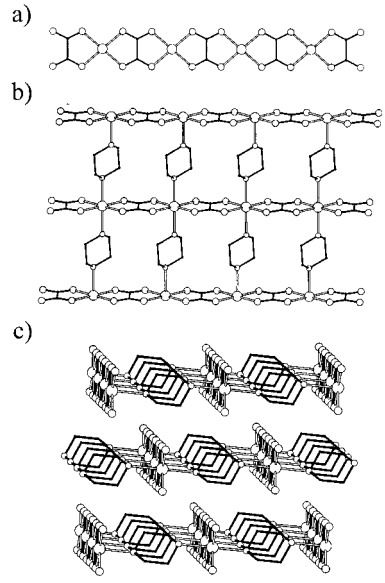

Figure 2. a) The symmetric oxalate bridging mode in the $[Ni(ox)]_\infty$ chains of **1**; b) the 2-D network formed by the intersection of metal-oxalate and metal-piperazine chains in **1**, viewed from an angle just off the *c*-axis; c) the packing of layers, viewed just off of the *a*-axis (hydrogen atoms omitted for clarity)

Table 2. Hydrogen bonds and short contacts: all hydrogen atom positions were fixed in an appropriate geometry and refined in riding mode

	D−H (Å)	H···A (Å)	D···A (Å)	D−H−A (°)
1				
N1−H1···O1[a]	0.910	2.67(2)	2.97(2)	100.4(3)
C2−H2b···O2[a]	0.970	2.47(1)	3.03(2)	116.7(3)
C1−H1a···O2	0.970	2.51(2)	2.99(2)	109.9(4)
C2−H2a···O2[b]	0.970	2.52(1)	3.28(2)	135.7(3)
C1−H1a···O1[c]	0.970	2.56(1)	3.31(1)	133.8(4)
2				
N2−H2···O2[d]	0.910	2.111(3)	2.904(5)	145.1(3)
N1−H1···O2[e]	0.910	2.158(3)	3.065(5)	175.1(3)
C5−H5a···O1[e]	0.971	2.398(3)	3.134(6)	132.2(3)
C5−H5a···O4[f]	0.971	2.453(3)	2.995(5)	114.9(3)
C3−H3b···O1	0.971	2.441(3)	2.981(6)	114.8(3)

[a] $-x, -y, -z$). [b] $(-x, -y, 1-z)$. [c] $(-x, -1-y, -z)$. [d] $(-1/2+x, 1/2-y, -z)$. [e] $(-x, 1/2+y, 1/2-z)$. [f] $(-1/2-x, 1-y, 1/2+z)$.

is through the bridging oxalate group, the next shortest Ni···Ni distances connect nickel ions in neighbouring layers along the *b* and *c* directions [5.9848(14) and 6.4997(16) Å, respectively]. The packing of these layers is shown in Figure 2 (c). There are several short C−H···O and N−H···O contacts between adjacent layers of Ni(pip)(ox) (Table 2). However, the very significant deviation from linearity of the N−H···O interaction and the fact that there are shorter C−H···O contacts suggests that hydrogen bonding to the amine proton is not significant in determining the overall structure of **1**.

The crystal structure of **2** contains one copper atom, one oxalate anion and one piperazine molecule in the asymmetric unit (Figure 3). The Cu^{II} cations are five-coordinate with a *trans*-N_2O_2 + O donor set in a square pyramidal geometry. The apical atom, O3, shows an elongated Cu−O bond of 2.413(3) Å, while the copper−ligand distances in the square base range from 1.954(3) to 2.060(4) Å. The oxalate anion bridges two neighbouring Cu atoms in an unsymmetrical manner, with one side of the oxalate unit in chelating mode through O1 (basal) and O3 (apical) while the other side is monodentate coordinating to a neighbouring copper atom through a basal site in a *syn*-geometry. This leaves one oxygen atom (O2) on the oxalate unit that is not involved in copper coordination. This oxalate bridging results in a polar ribbon of coplanar copper and oxalate ions running along the *c*-axis [Figure 4 (a)]. Within this ribbon, the copper ions form a zigzag chain with a Cu···Cu separation of 5.414(1) Å and a Cu−Cu−Cu angle of 158°. The piperazine molecule again adopts the low energy chair conformation with the hydrogen atoms on both nitrogen atoms, in an axial conformation. The piperazine groups also link neighbouring Cu atoms coordinating through *trans* sites on the square base of the pyramid to form a linear chain running parallel to the *a*-axis. Here the Cu···Cu separation is the *a*-parameter [6.8678(3) Å]. Together these two bridging units link copper ions into a 2-D array in the *ac*-plane [Figure 4 (b)]. Within a given layer all the $[Cu(ox)]_\infty$ chains have the same polarity, but between adjacent layers this polarity is reversed. Each amine proton is involved in hydrogen bonding to the oxygen atom O2 (not involved in copper coordination). In addition there are a large number of short C−H···O contacts (Table 2). The packing of these layers is shown in Figure 4 (c).

Although **1** and **2** have the same generic composition — M(pip)(ox) — the different stereoelectronic preferences of d^8 and d^9 configurations result in different metal coordination geometries and a change in the bridging mode of the oxalate. Despite these substantial local differences in the vicinity of the metal ions the overall structures show remarkable similarity. In both cases we can view the structures as intersecting chains of $[M(ox)]_\infty$ and $[M(pip)]_\infty$ resulting in a 2-D approximately "square" lattice of metal ions. These electrically neutral layers are then held together through a combination of Van der Waals and weak hydrogen bonding interactions.

Only three other nickel oxalate compounds display a linear chain motif; $[Ni(C_2O_4)(H_2O)_2]$,[7a−7c] [Ni(4-aminopyridine)$_2$(ox)][7d] and [Ni(4,4′-bipy)(ox)].[7e] The latter material

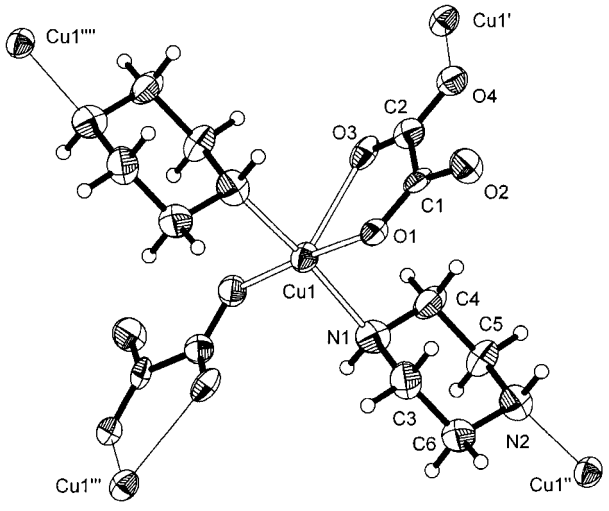

Figure 3. The asymmetric unit and selected symmetry equivalents of Cu(pip)(ox) (**2**) showing the copper coordination sphere and the bridging modes of both ligands; thermal ellipsoids are at the 90 % probability level; selected bond lengths (Å) and angles (°): Cu1−N1 2.058(4), Cu1−O1 1.954(3), Cu1−O3 2.413(3), Cu1′′−N2 2.043(4), Cu1′−O4 1.959(3), C1−C2 1.573(6), C1−O1 1.263(5), C1−O2 1.237(6), C2−O3 1.240(5), C2−O4 1.273(5) Å; N1−Cu1−O1 89.30(14), N1−Cu1−O4′′′′ 89.52(14), N2′′′′−Cu1−O4′′′ 90.65(14), N2′′′′−Cu1−O1 89.92(14), O3−Cu1−N1 99.55(15), O3−Cu1−O1 75.78(12), O3−Cu1−N2′′′′ 86.68(15), O3−Cu1−O4′′′ 109.54(12)°; symmetry codes: ′ ($^1/_2 - z$, $1 - y$, $-^1/_2 + z$); ′′ ($-1 + x$, y, z); ′′′ ($^1/_2 - x$, $1 - y$, $^1/_2 + z$); ′′′′ ($1 + x$, y, z).

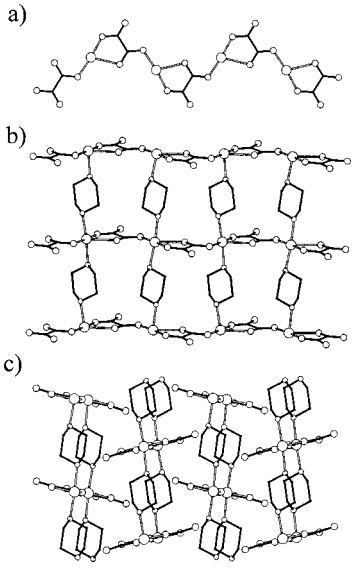

Figure 4. a) The unsymmetric oxalate bridging mode in **2**, resulting in a polar copper oxalate chain structure; b) the bridging mode of the oxalate ions and the linking of these chains by piperazine to form a 2-D net in **2**; view from just off the *b*-axis; c) the 3-D structure showing how layers pack together, viewed along the *c*-axis (hydrogen atoms omitted for clarity)

 © 2004 Wiley-VCH Verlag GmbH & Co. KGaA, Weinheim

displays remarkable structural similarity to **1** with essentially the same 2-D network topology. Other chain-containing materials are known where the oxalate ions coordinate to the nickel atom with *cis* geometry resulting in a zigzag chain structure.[7d,7f,7g] As with nickel, the majority of known compounds containing copper(II), oxalate and alkyl or aryl-amine ligands form dinuclear structures in which the oxalate-bridge metal ions in a symmetric bis-chelating fashion. However, there are a significant number of chain structures, which again contain bridging symmetric bis-chelating oxalate ions. Different amines have been used to stabilise linear chains[8a] (with *trans*-amine coordination), and zigzag chains[8b] (through *cis* coordination of the amine). Few copper(II) oxalate chain structures with a similar asymmetric oxalate bridging mode are known.[8c−8e] In all these cases the monodentate oxalate mode forms an axial coordination to the copper ion, resulting in a noncoplanar copper oxalate chain.

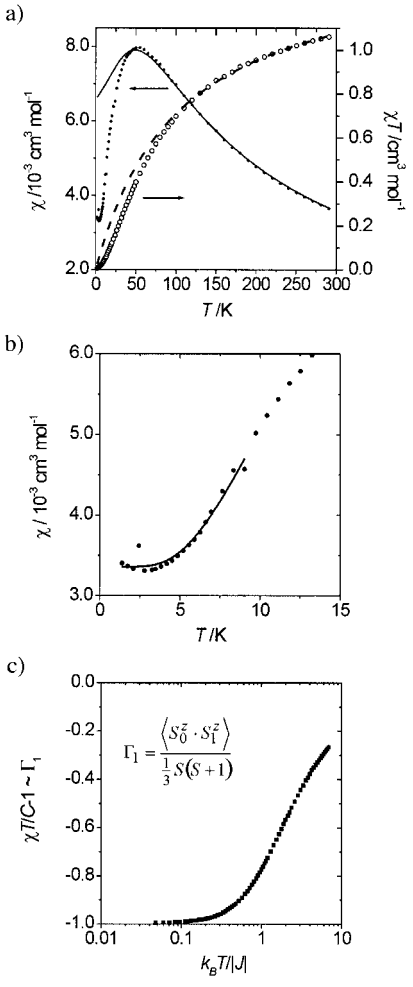

Figure 5. a) The thermal variation in the susceptibility (filled circles) of **1** and the best fit for an isotropic 1-D, (S = 1) model using Weng's equation for the data between 26 and 290 K; also shown in the product χT (open circles) and the Curie−Weiss fit to this data; b) fit of the low temperature data of **1** to an exponential function [Equation (3)] to estimate the energy gap; c) the nearest neighbour pair correlation function, Γ_1, derived from the susceptibility data plotted on a normalised axis scales

Electronic and Magnetic Properties

The approximately octahedral coordination of the Ni^{II} ion in **1** results in a $^3A_{1g}$ ground state, and the electronic spectra of **1** is consistent with this. We determined the crystal field splitting parameter, Δ_{oct} = 9440 cm^{-1}, the energy of the higher lying ^3P term to be at 11450 cm^{-1}, which results in β° = 27.7 %. We note also the presence of a spin-forbidden transition to a ^1E_g state at 14400 cm^{-1}. The enhanced intensity of this transition is due to mixing with the nearby $^3T_{1g}(F)$ state.

The magnetic susceptibility of **1** follows a Curie−Weiss law for data above 100 K [C = 1.446(7) $cm^3 \cdot K \cdot mol^{-1}$ and θ = −104(1) K]. A plot of $\mu_{eff}(T)$ shows the moment to increase monotonically on heating. It is clear that at the highest experimental temperature (290 K), the observed moment of 2.91 μ_B has not reached the asymptotic limit. A plot of $\chi(T)$ shows a broad maximum at 53(1) K with $\chi(T_{max})$ = 7.99(2) × $10^{-3} \cdot cm^3 \cdot mol^{-1}$ [Figure 5 (a)], on further cooling $\chi(T)$ tends to a value of 3.3(1) × 10^{-3} $cm^3 \cdot mol^{-1}$ as T approaches 0 K. The decrease in $\mu_{eff}(T)$ on cooling and the large negative Weiss constant suggest a significant antiferromagnetic exchange interaction between neighbouring nickel ions. From the crystallographic structure of **1** we expect the system to be well described as a 1-D "chain" of antiferromagnetically interacting spin moments. While typically spin-orbit coupling of the ground term to the low lying $^3T_{2g}$ state raises the g-value to about 2.25, g-values for Ni^{II} are usually isotropic, thus the system may be described by a Heisenberg Hamiltonian [Equation (1)]. The behaviour of an antiferromagnetically coupled chain of quantum spins was calculated by Weng,[10] and can be modelled by a polynomial approximation[11] [Equation (2)].

$$\hat{H} = -J \sum_i \mathbf{S}_i \cdot \mathbf{S}_{i+1} \tag{1}$$

$$\chi = \frac{N\mu_B^2 g^2}{k_B T}\left(\frac{A + Bx^2}{C + Dx + Ex^3}\right) \tag{2}$$

where $x = |J| / k_B T$

For $S = {}^1/_2$: A = 0.2500, B = 0.045743, C = 1.000, D = 0.77335, E = 0.43038

For S = 1: A = 0.6667, B = 0.64558, C = 1.000, D = 1.8018, E = 4.9448.

Least-squares fitting of the data over the whole of the measured temperature range (2−290 K) does not give a satisfactory agreement. The model underestimates the data at high temperatures and overestimates in the low temperature regime. If this model is applied to data over the limited region from 26 to 290 K a vastly improved fit is obtained [Equation (2); g = 2.31(1) and J/k_B = −42.2(3) K; Figure 5 (a)]. These couplings are in good agreement with reported values for a similarly bridged nickel oxalate compounds.[5,12]

 © 2004 Wiley-VCH Verlag GmbH & Co. KGaA, Weinheim

The discrepancy between the observed and calculated susceptibility at low temperatures may have one of several origins. Most likely either: a) the zero-field-splitting commonly observed in octahedral Ni^{II} complexes may be responsible; or b) we are seeing the formation of a "Haldane" quantum antiferromagnetic state. It is well-known that integer-spin chains are theoretically expected to display a gap[13] (known as the Haldane gap) immediately above a nonmagnetic ground state with novel quantum order. Theoretically this would result in an exponential increase in χ as T is increased from 0 K. In fact the low temperature susceptibility of **1** can be fitted to just such a model[14] [Equation (3); Figure 5 (b)] that results in a gap [Eg/k_B = 32(3) K]. This is in reasonable agreement with the expectation[15] that Eg is approximately $0.4|J|$ and is directly comparable to values reported for similarly coupled Ni^{II} chains.[16] We can use the measured susceptibility to derive an approximate value for the nearest-neighbour pair correlation function, Γ_1, from the susceptibility measurement.[17] The thermal evolution of Γ_1, which is proportional to the magnetic energy of the system, is shown in Figure 5 (c). For $\Gamma_1 = 0$ there is no correlation between neighbouring moments, while $\Gamma_1 = -1$ corresponds to perfect antiparallel alignment.

$$\chi = \chi_0 + C\exp\left(-\frac{Eg}{k_B T}\right) \tag{3}$$

The measured magnetic susceptibility of **2** shows a broad feature centred at about 13(2) K (determined by the derivative curve) although at the lowest experimental temperatures the susceptibility is seen to increase just as in a non-coupled paramagnetic material (Figure 6). A plot of reciprocal susceptibility vs. temperature showed approximately linear behaviour for data above 50 K. This could be fit to a Curie−Weiss law giving $C = 0.418(2)$ $cm^3 \cdot K \cdot mol^{-1}$ and $\theta = -44(1)$ K. The negative value for the Weiss constant θ, suggests a significant antiferromagnetic exchange interaction between neighbouring copper ions. From a plot of $\mu_{eff}(T)$, we can see that μ_{eff} increases on heating and by room temperature, the observed moment of 1.71(1) μ_B has not yet reached the asymptotic limit.

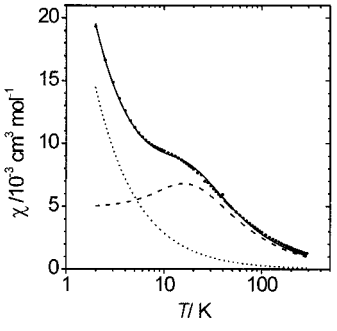

Figure 6. The thermal variation in the susceptibility (filled circles) of **2** and the best fit (solid line) for an isotropic 1-D, ($S = {}^1/_2$) model using Weng's equation plus a component due to a paramagnetic impurity (a logarithmic scale is used to highlight the good fit over a wide range of temperatures); each of these components is shown separately: contribution for **2** (dashed line), contribution due to paramagnetic impurity (dotted line)

Although consideration of the Cu···Cu separations suggests a 3-D network, the only likely magnetic superexchange pathway is through the bridging oxalate anion; thus we may anticipate 1-D magnetic behaviour. The observed broad maximum in the susceptibility at low temperature is consistent with this expectation. As with **1**, the magnetic interactions in compound **2** can be described by the Heisenberg Hamiltonian [Equation (1)], for which approximate solutions are known. Fitting the data to the quantum model[10,11] [Equation (2); Figure 6], plus a contribution due to a paramagnetic impurity gives a good fit [J/k_B = −25.9(1) K, g = 1.9 and 5.3 % paramagnetic impurity]. However, since the model clearly underestimates the high-temperature data it is likely that here g has been underestimated.

The coupling interaction between paramagnetic copper(II) ions is particularly well-studied, because the d^9 configuration always provides a simple spin ($S = {}^1/_2$) moment, free from orbital contributions and zero-field splitting effects which always complicate the analysis. Furthermore, the overwhelming tendency of Cu^{II} ions to form tetragonally elongated octahedra, square pyramid or square-planar coordination geometries results in a $d_{x^2-y^2}$ magnetic orbital and a clearly defined set of crystal field axis. The magnitude of the exchange coupling between Cu^{II} ions bridged by an oxalate ion depends crucially on the relative orientations of the magnetic $d_{x^2-y^2}$ orbitals of neighbouring cations and on the relative orientation of the oxalate group. Two different orbital orientations for the common symmetric bis-chelating mode are shown in Figure 7 (a and b).

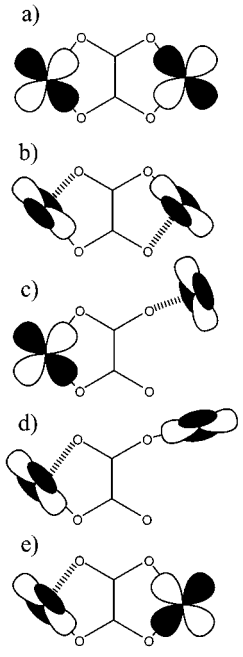

Figure 7. Some of the possible orbital topologies found in oxalato-bridged copper(II) compounds, see main text for details

 © 2004 Wiley-VCH Verlag GmbH & Co. KGaA, Weinheim

These different orbital topologies have antiferromagnetic couplings of approximately −500 and −9 K, respectively.[6,18] The unsymmetric μ-1,2,3-oxalato bridging mode is much less common[19] and in all previously reported compounds it appears that the magnetic orbital adopts the relative geometry shown in Figure 7 (c). This configuration supports exchange couplings in the range −0.50 to −3.9 K. To the best of our knowledge the disposition of the magnetic orbitals in **2** [Figure 7 (d)] is unique. This mode is related to an orbital topology seen occasionally in bis-chelating coordination geometries[8a,20] [Figure 7 (e)]. The larger exchange coupling observed in **2** compared to other unsymmetric μ-1,2,3 oxalato bridging modes is easily reconciled with the better spatial overlap of both metal $d_{x^2-y^2}$ orbitals and the oxalate orbitals.

Thermal Analysis

Thermogravimetric analysis of **1** under an O_2 atmosphere shows a single-stage decomposition at 400 °C to give a dark grey powder. The corresponding mass loss of 66.6 % agrees well with that expected upon formation of NiO. Compound **2** follows a similar single-step decomposition at about 220 °C with an observed weight loss of 38.9 %, consistent with the formation of CuO.

Conclusions

We have used two distinct bridging ligands to form a network with a topology that may have been anticipated. The difference in the structures of the Ni^{II} **1** and Cu^{II} **2** derivatives can be wholly attributed to the different stereoelectronic preferences of the d^8 and d^9 configurations. Both materials display 1-D antiferromagnetic behaviour consistent with the 1-D metal-oxalate structure. While the coupling constant in **1** is as expected the small value for **2** is due to the unusual orientations of the $d_{x^2-y^2}$ orbital on neighbouring metal ions relative to the oxalate bridge. The low temperature magnetism of **1** is consistent with the formation of a Haldane state, predicted for such a 1-D ($S = 1$) Heisenberg quantum antiferromagnet. However, these preliminary measurements do not rule out similar effects from zero-field splitting. If the low temperature state is a Haldane phase then **1** is an excellent material for further physical study. The fact that there is only one single spin carrier and one single coupling pathway per unit cell, and that both of these lie on crystallographic inversion centres greatly simplifies the interpretation of more sophisticated magnetic measurements. We are currently engaged in more detailed studies to better understand the magnetism of this ($S = 1$) material.

Experimental Section

Reagents: Nickel(II) hydroxide (97 %), oxalic acid (99 %), potassium oxalate monohydrate (99 %), and tetramethoxysilane (98 %) were all purchased from Aldrich, piperazine (99 %) from Acros, copper(I) chloride (96 %) from Fisher and copper(II) sulfate pentahydrate (99.5 %) from BDH. All used without further purification.

Physical Measurements: IR spectra were recorded on a Perkin−Elmer Spectrum One FT-IR machine as diffuse reflectance measurements between 4000 and 400 cm^{-1} using a KBr matrix. Elemental analysis for, C H and N was carried out commercially by Medac Ltd. UV-Vis/NIR spectra were recorded on a Perkin−Elmer Lambda 19 spectrometer in diffuse reflectance mode with the samples embedded in a $BaSO_4$ matrix. Thermogravimetric analysis was performed on a Metller Toledo TGA/SDTA851^e equipped with a T50800GCI gas control system and a T50801RD sample robot. Measurements were carried out under an atmosphere of approximately 60 % O_2 between 30 and 600 °C with a heating rate of 10 °C·min^{-1}. Single-crystal X-ray data was collected with monochromated Mo-K_α radiation (λ = 0. 71073 Å) on an Enraf−Nonius−Kappa CCD area detector as φ and ω scans to fill the Ewald sphere. Data collection and cell refinement were managed by DENZO,[21] absorption corrections were applied using SORTAV,[22] structure solution and refinement by SHELXS-97[23] and SHELXL-97[24] in the WinGX environment (Table 1).[25] CCDC-213878 **1** and CCDC-213879 **2** contain the supplementary crystallographic data for this paper. These data can be obtained free of charge at www.ccdc.cam.ac.uk/conts/retrieving.html [or from the Cambridge Crystallographic Data Centre, 12 Union Road, Cambridge CB2 1EZ, UK; Fax: (internat.) + 44-1223-336-033; E-mail: deposit@ccdc.cam.ac.uk].

Powder X-ray diffraction using a Siemens D5000 diffractometer was performed to confirm the purity and identity of all microcrystalline samples. Field-cooled magnetisation measurements were made between 2 and 290 K using a Quantum Design MPMS SQUID magnetometer in applied fields of 200 G. The powdered samples were held in an eicosane matrix to prevent reorientation effects. A diamagnetic correction of -119×10^{-6} cm^3·mol^{-2} was determined from Pascal's constants[26] and applied to both samples.

Synthesis of Ni(pip)(ox) (1): Nickel hydroxide (100 mg, 1.07 mmol), oxalic acid dihydrate (254 mg, 2.25 mmol), piperazine (689 mg, 8.00 mmol) and distilled water (10 mL) were placed into a 23 mL capacity Teflon lined autoclave and heated to 180 °C under autogenous pressure for 72 h. The green microcrystalline product was collected by filtration and dried in air (30 mg, 12 %). $C_6H_{10}N_2NiO_4$ (232.9): C 30.95, H 4.33, N 12.03; found C 31.23, H 4.61, N 12.08. IR: $\tilde{\nu}$ = 3250 cm^{-1} m, 3108 w, 3072 w, 3004 m, 2975 w, 2918 m, 2880 m, 2825 w, 2679 w, 2554 w, 2509 w, 2420 w, 2420 w, 2274 w, 2031 w, 1972 w, 1895 w, 1619 s, 1457 s, 1439 m, 1420 s, 1362 m, 1342 m, 1314 s, 1249 m, 1098 m, 1069 s, 1019 s, 992 s, 905 m, 881 s, 804 s, 647 m, 488 s, 414 s. UV-Vis: λ_{max} /cm^{-1} (ε/relative) = 9500 (0.423) $^3A_{2g} \rightarrow {}^3T_{2g}$(F), 14400 (0.315) $\rightarrow {}^1E_g$, 15600 (0.292) $\rightarrow {}^3T_{1g}$(F), 24700 (0.162) $\rightarrow {}^3T_{2g}$(P), 37900 (1.000).

Synthesis of Cu(pip)(ox) (2): A mixture of copper(I) chloride (1.000 g, 10.10 mmol), potassium oxalate monohydrate (2.000 g, 10.86 mmol), piperazine (1.000 g, 11.61 mmol) and distilled water (15 mL) was allowed to react in air for a period of 6 days. During the course of the reaction Cu^I both disproportionates and is slowly oxidised by air to Cu^{II}. The product is formed as a purple precipitate. The major contaminant $K_2Cu(ox)_2$·$2H_2O$ is removed by dissolution in H_2O and the product is collected by filtration. Yield 85 %. $C_6H_{10}CuN_2O_4$ (237.7): calcd. C 30.32, H 4.24, N 11.78; found C 28.54, H 4.44, N 10.81. IR: $\tilde{\nu}$ = 3189 cm^{-1} s, 3167 s, 2996 m, 2950 m, 2884 m, 2798 m, 2379 w, 2191 w, 1657 s, 1631 s, 1606 s, 1443 m, 1372 m, 1347 m, 1306 s, 1239 m, 1151 s, 1092 s, 1028 m, 1008 m, 892 s, 833 m, 789 s, 675 m, 596 m, 517 s, 421 m. UV-Vis: λ_{max} /cm^{-1} (ε/relative) = 14700 (0.684), 17500 (0.772), 27000 (0.930), 29100 (0.965), 33800 (1.000).

 © 2004 Wiley-VCH Verlag GmbH & Co. KGaA, Weinheim

Crystallisation of 2: Single crystals of **2** were obtained by a gel crystallisation method. Tetramethoxysilane (2 mL) was added to a solution of piperazine (0.500 g, 5.81 mmol) and potassium oxalate monohydrate (1.00 g, 5.43 mmol) in distilled water (18 mL), and the mixture allowed to react. This gel was transferred to a test tube. A solution of copper sulfate pentahydrate (1.25 g, 4.81 mmol) in distilled water (5 mL) was added to the top and allowed to diffuse slowly into the gel. After three days small, purple crystals of **2** formed.

Acknowledgments

We are grateful to Dr. H. J. Blythe (The University of Sheffield) for assistance with the magnetisation measurements and Dr. A. L. Hector (University of Southampton) for measurement of the TGA data. D. J. P. thanks the EPSRC for the award of an Advanced Research Fellowship.

[1] [1a] T. O. Salami, K. Marouchkin, P. Y. Zavillij, S. R. J. Oliver, *Chem. Mater.* **2002**, *14*, 4851. [1b] R. Vaidhyanathan, S. Natarajan, C. N. R. Rao, *J. Chem. Soc., Dalton Trans.* **2001**, 699. [1c] R. Vaidhyanathan, S. Natarajan, A. K. Cheetham, C. N. R. Rao, *Chem. Mater.* **1999**, *11*, 3636. [1d] S. Natarajan, R. Vaidhyanathan, C. N. R. Rao, S. Ayyappan, A. K. Cheetham, *Chem. Mater.* **1999**, *11*, 1633. [1e] S. Ayyappan, A. K. Cheetham, S. Natarajan, C. N. R. Rao, *Chem. Mater.* **1998**, *10*, 3746.

[2] Z. A. D. Lethbridge, A. F. Congreve, E. Esslmont, A. M. Z. Slawin, P. Lightfoot, *J. Solid State Chem.* **2003**, *172*, 212.

[3] [3a] P. Rabu, M. Drillon, *Adv. Eng. Mater.* **2003**, *5*, 189 and the references therein. [3b] S. Natarajan, *Solid State. Sci.* **2003**, *4*, 1331. [3c] R. Pellaux, H. W. Schmalle, R. Huber, P. Fischer, T. Hauss, B. Ouladdiaf, S. Decurtins, *Inorg. Chem.* **1997**, *36*, 2301. [3d] S. Decurtins, H. W. Schmalle, H. R. Oswald, A. Linden, J. Ensling, P. Gütlich, A. Hauser, *Inorg. Chim. Acta* **1994**, *216*, 65.

[4] [4a] R. Clément, S. Decurtins, M. Gruselle, C. Train, *Monats. Chem.* **2003**, *134*, 117 and references therein. [4b] E. Coronado, J. R. Galan-Mascaros, C. J. Gomez-Garcia, J. M. Martinez-Agudo, *Inorg. Chem.* **2001**, *40*, 113. [4c] K. P. Mortl, J.-P. Sutter, S. Golhen, L. Ouahab, O. Kahn, *Inorg. Chem.* **2000**, *39*, 1626. [4d] R. Andres, M. Gruselle, B. Malezieux, M. Verdaguer, J. Vaissermann, *Inorg. Chem.* **1999**, *38*, 4637. [4e] S. Decurtins, *Phil. Trans. Roy. Soc. Sect A* **1999**, *357*, 3025 and references therein.

[5] [5a] A. Escuer, R. Vicente, J. Ribas, J. Jaud, B. Raynaud, *Inorg. Chim. Acta* **1994**, *216*, 139. [5b] P. Román, C. Guzmán-Miralles, A. Luque, J. I. Beitia, J. Cano, F. Lloret, M. Julve, S. Alvarez, *Inorg. Chem.* **1996**, *35*, 3741. [5c] R. Wen, I. Bernal, S. S. Massoud, R. K. Thalji, D. R. Billodeaux, F. R. Fronczek, *Inorg. Chim. Acta* **1999**, *295*, 91.

[6] J. Cano, E. Ruiz, P. Alemany, F. Lloret, S. Alvarez, *J. Chem. Soc., Dalton Trans.* **1999**, 1669.

[7] [7a] H. Schmittler, *Monats. Dtsch. Akad. Wiss. Ber.* **1967**, *9*, 445. [7b] J.-P. Lagier, H. Pezerat, J. Dubernat, *Rev. Chim. Miner.* **1969**, *6*, 1081. [7c] R. Deyrieaux, C. Berro, A. Peneloux, *Bull. Soc. Chim. Fr.* **1973**, 25. [7d] O. Castillo, A. Luque, P. Román, F. Lloret, M. Julve, *Inorg. Chem.* **2001**, *40*, 5526. [7e] J. Y. Lu, M. A. Lawandy, J. Li, T. Yuen, C. L. Lin, *Inorg. Chem.* **1999**, *38*, 2695. [7f] O. Castillo, A. Luque, F. Lloret, P. Román, *Inorg. Chim. Acta* **2001**, *324*, 141. [7g] J. Y. Lu, T. J. Schrieder, A. M. Babb, M. Olmstead, *Polyhedron* **2001**, *20*, 2445.

[8] [8a] O. Castillo, A. Luque, F. Lloret, P. Román, *Inorg. Chem. Commun.* **2001**, *4*, 350. [8b] O. Castillo, A. Luque, M. Julve, F. Lloret, P. Román, *Inorg. Chim. Acta* **2001**, *315*, 9. [8c] J. Novosad, A. C. Messimeri, C. D. Papadimitriou, P. G. Veltsistas, J. D. Woolins, *Transition Met. Chem.* **2000**, *25*, 664. [8d] H. Oshio, U. Nagashima, *Inorg. Chem.* **1992**, *31*, 3295. [8e] U. Geiser, B. L. Ramakrishna, R. D. Willett, F. B. Hulsbergen, J. Reedijk, *Inorg. Chem.* **1987**, *26*, 3750.

[9] [9a] L. Cavalca, A. C. Vila, A. G. Manfredotti, A. A. G. Tomlinson, *J. Chem. Soc., Dalton Trans.* **1972**, 391. [9b] M. R. Sundberg, R. Kivekas, J. K. Koskimies, *J. Chem. Soc., Chem. Commun.* **1991**, 526. [9c] M. Hernandez-Molina, P. A. Lorenzo-Luiz, C. Ruiz-Perez, *Cryst. Eng. Commun.* **2001**, 16.

[10] C. Y. Weng, *PhD Thesis*, Carneige-Mellon University, Pittsburg, PA, **1969**.

[11] W. Hiller, J. Strähle, A. Datz, M. Hanack, W. E. Hatfield, L. E. ter Haar, P. Gütlich, *J. Am. Chem. Soc.* **1984**, *106*, 329.

[12] [12a] J. Glerup, P. A. Goodson, D. J. Hodgson, K. Michelsen, *Inorg. Chem.* **1995**, *34*, 6255. [12b] F. Brezina, Z. Smekal, Z. Travnicek, Z. Sindelar, R. Pastorek, J. Marek, *Polyhedron* **1997**, *16*, 1331. [12c] Z. Smekal, P. Thornton, Z. Sindelar, R. Klicka, *Polyhedron* **1998**, *17*, 1631. [12d] R. W. Wen, I. Bernal, S. S. Massoud, R. K. Thalji, D. R. Billodeaux, F. R. Fronczek, *Inorg. Chim. Acta* **1999**, *295*, 91. [12e] I. Muga, J. M. Gutiérrez-Zorrilla, P. Vitoria, A. Luque, M. Insausti, P. Román, F. Lloret, *Eur. J. Inorg. Chem.* **2000**, 2541.

[13] [13a] F. D. Haldane, *Phys. Lett. Sect A* **1983**, 464. [13b] F. D. Haldane, *Phys. Rev. Lett.* **1983**, *50*, 1153.

[14] T. Ishii, N. Aizawa, H. Hara, M. Yamashita, H. Matsuzaka, *Polyhedron* **2001**, *20*, 1297.

[15] M. P. Nightingale, H. W. J. Blöte, *Phys. Rev. B.* **1986**, *33*, 659.

[16] M. S. El Fallah, A. Escuer, R. Vicente, X. Solans, M. Font-Bardia, M. Verdaguer, *Inorg. Chim. Acta* **2003**, *344*, 133.

[17] L. J. de Jongh, A. R. Miedema, *Adv. Phys.* **2001**, *50*, 947.

[18] [18a] J. J. Girerd, O. Kahn, M. Verdauger, *Inorg. Chem.* **1980**, *19*, 274. [18b] O. Castillo, I. Muga, A. Luque, J. M. Gutiérrez-Zorrilla, J. Sertucha, P. Vitoria, P. Román, *Polyhedron* **1999**, *18*, 1235. [18c] J. Cano, P. Alemany, S. Alvarez, M. Verdaguer, E. Ruiz, *Chem. Eur. J.* **1998**, *4*, 476.

[19] H. Núñez, J.-J. Timor, J. Server-Carrió, L. Soto, E. Escrivà, *Inorg. Chim. Acta* **2001**, *318*, 8 and references therein.

[20] [20a] M. Julve, M. Verdaguer, O. Kahn, A. Gleizes, O. Philoche-Levisalles, *Inorg. Chem.* **1984**, *23*, 3808. [20b] S. Kitagawa, T. Okubo, S. Kawata, M. Kondo, M. Katada, H. Kobayashi, *Inorg. Chem.* **1995**, *34*, 4790.

[21] Z. Otwinoski, W. Minor, in *Methods in Enzymology*, vol. 276: *Macromolecular Crytstallography* (Eds.: C. W. Carter Jr., R. M. Sweet), Academic Press, **1997**, *Part A*, p. 307.

[22] [22a] R. H. Blessing, *Acta Crystallogr., Sect. A* **1995**, 33. [22b] R. H. Blessing, *J. Appl. Cryst.* **1997**, *30*, 421.

[23] G. M. Sheldrick, *Acta Crystallogr., Sect. A* **1990**, 467.

[24] G. M. Sheldrick, University of Göttingen, Germany, **1997**.

[25] L. J. Farrugia, *J. Appl. Cryst.* **1999**, *32*, 837.

[26] O. Kahn, *Molecular Magnetism*, VCH, Weinheim, **1993**.

Received August 22, 2003
Early View Article
Published Online January 28, 2004

 © 2004 Wiley-VCH Verlag GmbH & Co. KGaA, Weinheim